

AD-A092 588

NAVAL RESEARCH LAB WASHINGTON DC

F/6 20/9

LINEAR STABILITY OF SELF-SIMILAR FLOW. 8. IMPLoding CYLINDRICAL--ETC(U)

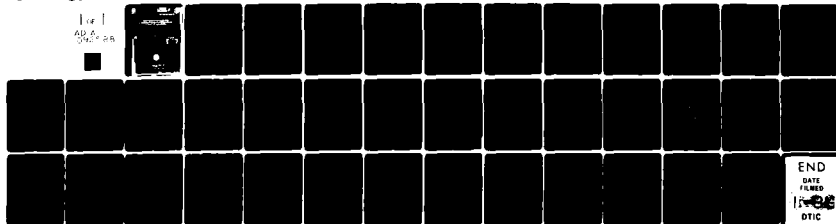
OCT 80 J H GARDNER, D L BOOK, I B BERNSTEIN

UNCLASSIFIED

NRL-MR-4370

NL

1 of 1
AD-A092 588



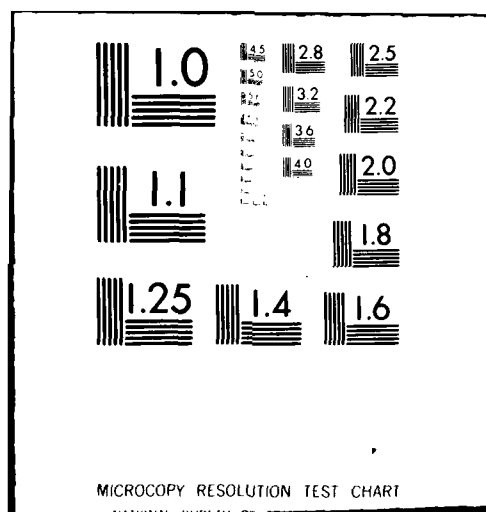
END

DATE

FILED

1980

DTIC



AD A092588

9 REPORT DOCUMENTATION PAGE		READ INSTRUCTIONS BEFORE COMPLETING FORM
1. REPORT NUMBER NRL Memorandum Report, 1370	2. GOVT ACCESSION NO. AD-A092	3. RECIPIENT'S CATALOG NUMBER 588
4. TITLE (and Subtitle) A083918 LINEAR STABILITY OF SELF-SIMILAR FLOW. 8. IMPLODING CYLINDRICAL AND SPHERICAL SHOCKS IN THE C-C-W APPROXIMATION.		5. TYPE OF REPORT & PERIOD COVERED Interim report on a continuing NRL problem.
7. AUTHOR(s) 10 John H. Gardner, David L. Book and Ira B. Bernstein		6. PERFORMING ORG. REPORT NUMBER
9. PERFORMING ORGANIZATION NAME AND ADDRESS Naval Research Laboratory Washington, DC 20375		8. CONTRACT OR GRANT NUMBER(s) 11 34 Oct 80
11. CONTROLLING OFFICE NAME AND ADDRESS Department of Energy Washington, DC 20585		10. PROGRAM ELEMENT, PROJECT, TASK AREA & WORK UNIT NUMBERS 62-0575-0-0
14. MONITORING AGENCY NAME & ADDRESS (if different from Controlling Office) 14 N+L-M-437A		12. REPORT DATE October 31, 1980
		13. NUMBER OF PAGES 38
		15. SECURITY CLASS. (of this report) UNCLASSIFIED
		15a. DECLASSIFICATION/DOWNGRADING SCHEDULE
16. DISTRIBUTION STATEMENT (of this Report) Approved for public release; distribution unlimited.		
17. DISTRIBUTION STATEMENT (of the abstract entered in Block 20, if different from Report)		
18. SUPPLEMENTARY NOTES *Present address: Department of Engineering and Applied Sciences Yale University This research was supported by the U. S. Department of Energy.		
19. KEY WORDS (Continue on reverse side if necessary and identify by block number) Shock waves ICF Stability Laser targets Implosions Pellet		
20. ABSTRACT (Continue on reverse side if necessary and identify by block number) Analytical and computational techniques are developed to investigate the stability of converging shock waves in cylindrical and spherical geometry. The linearized Chester-Chisnell-Whitham (C-C-W) equations describing the evolution of an arbitrary perturbation about an imploding shock wave in an ideal fluid are solved exactly in the strong-shock limit for a density profile $\rho(r)$. All modes are found to be relatively unstable (i.e., the ratio of perturbation amplitude to shock radius diverges as the latter goes to zero), provided that q is not too large. and APPROX (Continues)		

20. Abstract (continued)

The nonlinear C-C-W equations are solved numerically for both moderate and strong shocks. The small-amplitude limit agrees with the analytical results, but some forms of perturbation which are stable at small amplitude become unstable in the nonlinear regime. The results are related to the problem of pellet compression in experiments on inertial confinement fusion.

CONTENTS

I. INTRODUCTION	1
II. MODEL EQUATIONS	4
III. LINEARIZED ANALYTIC SOLUTIONS	6
IV. NUMERICAL INTEGRATIONS	12
V. COMPARISON OF RESULTS OF LINEARIZED MODEL AND NONLINEAR INTEGRATION	16
VI. NONLINEAR MODELING	22
VII. EFFECT OF DENSITY VARIATION	29
VIII. CONCLUSIONS	34
REFERENCES	35

Accession For	
NTIS GRA&I	<input checked="checked" type="checkbox"/>
DDC TAB	<input type="checkbox"/>
Unannounced	<input type="checkbox"/>
Justification	
By _____	
Distribution/ _____	
Availability Codes	
Dist	Avail and/or special
A	

LINEAR STABILITY OF SELF-SIMILAR FLOW:
8. IMPLODING CYLINDRICAL AND SPHERICAL SHOCKS
IN THE C-C-W APPROXIMATION

I. Introduction

One of the critical limitations to achieving high compression in a spherical implosion is the degree of symmetry that can be maintained. This in turn has important implications for target fabrication techniques and for laser or other driver designs, since it establishes the tolerances required in the symmetry of these components.

An important issue for understanding imploding systems is the stability of a converging shock wave. This shock wave might be used, for instance, not only to compress the fuel, but also to provide the heating required to create a central ignition region. The final temperature achieved will depend on how nearly spherical the shock wave remains during the collapse process and the shape of the shock at the time of reflection.

A certain inherent stability of a shock wave results from the well-known fact that a shock wave with a smaller radius of curvature advances faster than one with a larger radius of curvature. Thus, the part of a perturbed shock front that initially lags behind will accelerate more rapidly due to its smaller radius of curvature and so will tend to catch up with the remainder of the shock wave. However, the perturbation may be unable to overtake the main shock, which is accelerating because of convergence, or it may be overdriven, i.e., the perturbation may overshoot the stable position.

In order to discuss stability, it is necessary to define what is meant by stable (or unstable) behavior. The usual definition of stability in

Manuscript submitted September 16, 1980.

terms of a growing or decaying mode amplitude does not adequately describe the situation in imploding systems. For example, the amplitude may not tend to zero as fast as the average radius, or the collapse time may be of the order of the period of oscillation of the mode. A more meaningful number for small-amplitude perturbations is the rate of growth (or decay) of the relative perturbation amplitude, i.e., the ratio of the perturbation amplitude to the radius of the zero-order symmetric collapse solution (Bernstein and Book, 1978).

Large initial perturbation amplitudes may not decay in the same way as small-amplitude perturbations (Fong and Ahlborn, 1979). One can define a radial instability in terms of the maximum deviation of the shock radius from the average radius ($|R - R_{ave}|/R_{ave}$). Another kind of instability (kink instability) occurs when a small portion of the shock necks off from the central region (Fig. 1). In general, we cannot speak of an imploding shock as being stable or unstable in a clear-cut sense. Rather, we can ask whether it retains an acceptable degree of symmetry after having collapsed to a volume sufficiently small for practical purposes.

We have developed an analytic and computational model to investigate the stability of converging shock waves in cylindrical and spherical geometry. This represents an extension to smaller radii of the work of Fong and Ahlborn (1979) on the linear stability problem. The model equations are described in the next section, followed by a linearized analytic solution, an account of the numerical model, a comparison of the numerical and analytic solutions, an analysis of nonlinear behavior, and an extension to problems with a varying density in front of the shock.

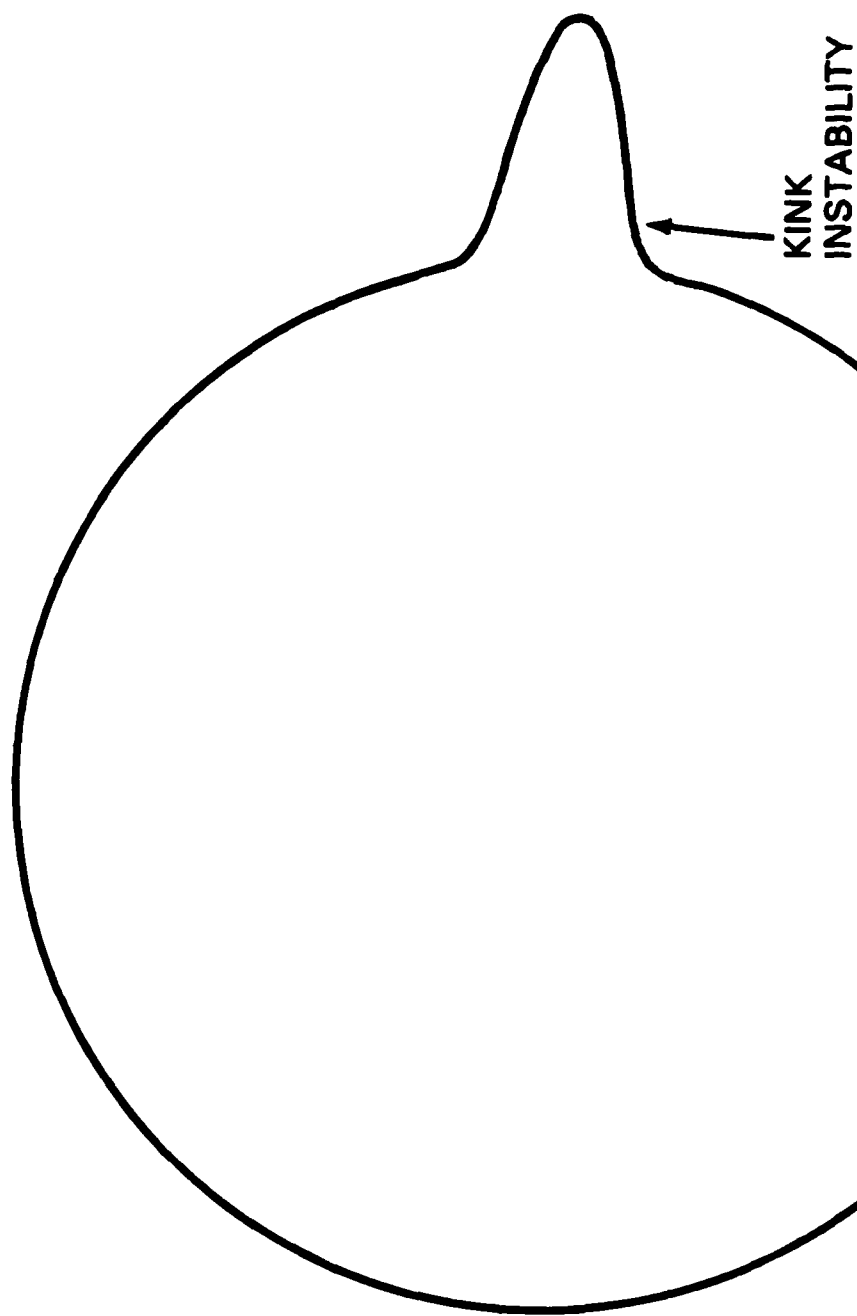


Fig. 1 — Kink instabilities form when the main shock accelerates due to spherical convergence ahead of a perturbed portion of the shock which is unable to catch up in spite of its smaller radius of curvature.

II. Model Equations

The motion of a converging shock wave can be computed with great accuracy by considering only changes in the physical variables across the shock front, ignoring the fluid motion behind the shock surface. The velocity of a shock front in a motionless undisturbed medium is normal to the front. It may therefore be treated as a locally one-dimensional motion in a channel whose boundaries are determined by the trajectories of the shock front. These trajectories form imaginary ray tubes whose cross-sectional area is related to the Mach number by an equation derived by Chester (1954), Chisnell (1955), and Whitham (1957) (the C-C-W approximation). The equation may be found by substituting into the compatibility equation for the characteristic moving in the direction of shock propagation the fluid quantities determined by the Rankine-Hugoniot relations across the shock. Whitham (1958) has shown that this procedure, the simplest method of deriving the C-C-W approximation, is equivalent to solving the complete fluid equations while ignoring the characteristics which travel away from the shock and are reflected back toward it. For this reason, it is most accurate for accelerating shocks, where the reflected characteristics are unable to catch up with the shock.

The result of this model is an equation for the Mach number M of the shock as a function of the cross-sectional area A of the ray tube:

$$\frac{\lambda(M)M dM}{M^2 - 1} + \frac{dA}{A} = 0, \quad (1)$$

where

$$\lambda(M) = (2\sigma + 1 + 1/M^2) \left(1 + \frac{2}{\gamma + 1} \frac{1 - \sigma^2}{\sigma}\right), \quad (2)$$

and

$$\sigma^2 = \frac{(\gamma - 1)M^2 + 2}{2\sigma M^2 - (\gamma - 1)}, \quad (3)$$

where γ is the usual adiabatic index. The cross-sectional area of the ray tube may be expressed in terms of the shock front velocity by the kinematic relations

$$\dot{A} = -A \underline{\underline{n}} \cdot (\underline{\underline{n}} \times \nabla) \times \underline{\underline{v}} \quad (4)$$

$$\dot{\underline{\underline{n}}} = - (\underline{\underline{I}} - \underline{\underline{n}}\underline{\underline{n}}) \cdot (\underline{\underline{n}} \times \underline{\underline{v}}) \times \underline{\underline{v}}; \quad (5)$$

$$\dot{\underline{\underline{r}}} = \underline{\underline{v}} = \underline{\underline{n}} v, \quad (6)$$

where $(\dot{})$ denotes a derivative with respect to time, $\underline{\underline{n}}$ is the unit vector normal to the shock front and $\underline{\underline{r}}$ is the surface location.

In numerical integration, Eqs. (1) and (5) are used to propagate the magnitude and direction, respectively, of the shock front velocity in terms of time, substituting \dot{A} from Eq. (4). Equation (6) then advances the shock front position by integration of the velocity. For small perturbations about symmetric (cylindrical or spherical) shocks, however, solutions can be obtained analytically.

III. Linearized Analytic Solutions

Since all collapsing shocks will eventually become strong, it is useful to analyze the strong shock limit $M \gg 1$. If we assume that the sound speed ahead of the shock is constant, in addition to being small, then Eqs. (1)-(3) reduce to

$$\dot{A}/A = -\lambda \dot{v}/v, \quad (7)$$

where

$$v = M/a \quad (8)$$

and

$$\lambda = \frac{\gamma+2}{\gamma} + \left(\frac{2\gamma}{\gamma-1}\right)^{1/2}, \quad (9)$$

Using familiar vector identities we have

$$\underline{n} \cdot (\underline{n} \times \nabla) \times \underline{v} = -v \nabla \cdot \underline{n} \quad (10)$$

Thus using Eqs. (4) and (7)-(10) we have

$$(\lambda/v)' = \nabla \cdot \underline{n} = \underline{n} \times (\underline{n} \times \nabla) \cdot \underline{n}, \quad (11)$$

which only involves tangential derivatives of \underline{n} .

We first look at the zeroth-order symmetric solution,

$$\dot{r} = v(t); \quad (12)$$

$$\underline{n} = \underline{e}_r; \quad (13)$$

$$\dot{\underline{n}} = 0; \quad (14)$$

$$(\lambda/\dot{r})' = \nabla \cdot (\underline{r}/r) = \alpha/r, \quad (15)$$

where $\alpha = 1$ (2) for cylindrical (spherical) geometry. Equations

(12)-(15) can be rewritten as

$$\dot{r} \frac{d}{dr} (\lambda/\dot{r}) = -\lambda \frac{d}{dr} \ln \dot{r} = \frac{\alpha}{r} = \frac{d}{dr} \ln r^\alpha. \quad (16)$$

Integrating this once yields

$$\dot{r} r^{\alpha/\lambda} = \text{const}, \quad (17)$$

and finally

$$r = R (\omega t)^{\lambda/(\lambda+\alpha)}, \quad (18)$$

where R and ω are constants.

Suppose we now linearize the equation by assuming $\underline{n} = \underline{n}_0 + \underline{n}_1$, $\underline{v} = \underline{v}_0 + \underline{v}_1$, $\underline{r} = \underline{r}_0 + \underline{\xi}(\underline{r}_0, t)$, where the subscript 0 refers to the zeroth-order symmetric solution, and the subscript 1 refers to a small perturbation about this solution. From Eq. (5) we have

$$\underline{n}_1 = - (\underline{I} - \underline{n}_0 \underline{n}_0) \cdot (\underline{n}_0 \times \nabla_0) \times \underline{\xi} \quad (19)$$

Expanding the gradient operator

$$\nabla = \nabla_0 - (\nabla_0 \underline{\xi}) \cdot \nabla_0 + \dots, \quad (20)$$

from Eq. (11) we have to first order

$$(-\lambda v_1 / v_0^2) \cdot = \nabla_0 \cdot \underline{n}_1 - (\nabla_0 \underline{\xi}) : (\nabla_0 \underline{n}_0). \quad (21)$$

From Eq. (19) after some manipulation we have

$$\underline{n}_1 - \underline{\xi} \cdot \nabla_0 \underline{n} = - (\underline{I} - \underline{n}_0 \underline{n}_0) \cdot \nabla_0 (\underline{n}_0 \cdot \underline{\xi}) \quad (22)$$

Here use has been made of the fact that $\underline{n}_0 = \underline{e}_r$ and the fact that

$$\nabla_0 \underline{n}_0 = \nabla_0 (\underline{r}_0 / r_0) = (\underline{I} - \underline{n}_0 \underline{n}_0) / r_0 \quad (23)$$

is a symmetric dyad. From Eq. (6) we have

$$\dot{\underline{\xi}} = \underline{n}_0 v_1 + \underline{n}_1 v_0 \quad (24)$$

Hence taking the dot product with \underline{n}_0 yields

$$\underline{n}_0 \cdot \dot{\underline{\xi}} = (\underline{n}_0 \cdot \underline{\xi}) \cdot = v_1 \quad (25)$$

Thus Eq. (21) can be written as

$$\begin{aligned} \left(\frac{\lambda \underline{n}_0 \cdot \dot{\underline{\xi}}}{v_0^2} \right) &= \nabla_0 [\underline{n}_1 - \underline{\xi} \cdot \nabla_0 \underline{n}_0] + \underline{\xi} \cdot \nabla_0 \nabla_0 \cdot \underline{n}_0 \\ &= - \nabla_0 \cdot [(\underline{I} - \underline{n}_0 \underline{n}_0) \cdot \nabla_0 (\underline{n}_0 \cdot \underline{\xi})] + \underline{\xi} \cdot \nabla_0 \left(\frac{\underline{\alpha}}{r_0} \right). \end{aligned} \quad (26)$$

Now if we expand the perturbation in either cylindrical or spherical harmonics by assuming a sum of linearly independent terms of the form

$$\underline{n}_0 \cdot \underline{\xi} = \zeta(t) \cos(m\varphi) \quad (\text{cylindrical}) \quad (27)$$

$$= \zeta(t) P_l^m \cos(m\varphi) \quad (\text{spherical}), \quad (27')$$

each of which can be treated independently, and define the mode-number-dependent coefficient of the Laplacian by

$$\begin{aligned}
 Q &= m^2 & (\text{cylindrical}) & (28) \\
 &= \ell(\ell+1) & (\text{spherical}), & (28')
 \end{aligned}$$

Eq. (26) becomes

$$-(\lambda \dot{\zeta}/v_0^2) = \zeta(Q-\alpha)/r_0 \quad (29)$$

Now using

$$\dot{\zeta} = v_0 \frac{d\zeta}{dr_0} \quad (30)$$

we have

$$v_0 \frac{d}{dr_0} \left[(\lambda/v_0) \frac{d\zeta}{dr_0} \right] = \frac{\alpha - Q}{r_0^2} \zeta \quad (31)$$

From Eq. (18) we have

$$\frac{d \ln v_0}{dr_0} = -\frac{\alpha}{\lambda r_0} \quad (32)$$

and after a little algebraic manipulation we get

$$\lambda \frac{d^2 \zeta}{dr_0^2} + \frac{\alpha}{r_0} \frac{d\zeta}{dr_0} + \frac{Q - \alpha}{r_0^2} \zeta = 0. \quad (33)$$

We now seek a solution of the form $\zeta \sim r_0^\beta$, where β is in general a complex number which satisfies the indicial equation

$$\lambda \beta(\beta-1) + \alpha \beta + Q - \alpha = 0, \quad (34)$$

or

$$\beta = \frac{1}{2\lambda} \{ \lambda - \alpha \pm [(\lambda + \alpha)^2 - 4\lambda Q]^{1/2} \}. \quad (35)$$

Since we seek the ratio of the amplitude of the disturbance to that of the zeroth order solution we look at

$$\zeta/r_0 = r_0^{\beta-1} = r_0^{\{ -(\lambda + \alpha) \pm [(\lambda + \alpha)^2 - 4\lambda Q]^{1/2} \} / 2\lambda} \quad (36)$$

Since

$$r_0 \sim r \frac{\lambda}{\lambda + \alpha} \quad (37)$$

$$\zeta/r_0 \sim t^{-\frac{1}{2} \pm [(\lambda + \alpha)^2 - 4 \lambda Q]^{\frac{1}{2}} / 2(\lambda + \alpha)} \quad (38)$$

For the lowest-order mode numbers $\beta - 1$ is real and negative, indicating that the disturbance is geometrically unstable:

$$\beta - 1 = - \frac{\lambda + \alpha}{\lambda}, 0 \quad (39)$$

for $l=0$ (spherical coordinates) or $m=0$ (cylindrical coordinates), and

$$\beta - 1 = - \frac{\alpha}{\lambda}, -1 \quad (40)$$

for $l=1$ (spherical coordinates) or $m=1$ (cylindrical coordinates).

For all mode numbers greater than unity β is complex, and there is a factor growing with a power-law dependence $\sim r_0^{-(\lambda + \alpha)/(2\lambda)}$ and a factor which is oscillatory in $\ln r_0$ with a frequency $\omega = \frac{1}{2\lambda} [4\lambda Q - (\lambda + \alpha)^2]^{\frac{1}{2}}$. The real part is always negative and independent of mode number, while the oscillatory part depends on the mode number:

$$\zeta/r_0 \sim r_0^{-\frac{\lambda + \alpha}{2\lambda} \pm i \frac{\lambda + \alpha}{\lambda} p}, \quad (41)$$

where

$$p = \frac{[4\lambda Q - (\lambda + \alpha)^2]^{\frac{1}{2}}}{2(\lambda + \alpha)}. \quad (42)$$

In Fig. 2 we show the frequency in $\ln t$ for the spherical harmonic perturbation as a function of mode number for two different ratios of specific heat, $\gamma = 7/5$ and $\gamma = 5/3$. Figure 3 shows the ratio r/r_0 between successive minima in the perturbation amplitude as it oscillates during collapse. The ratio may be chosen so that at some prescribed degree of compression the perturbation amplitude is a minimum.

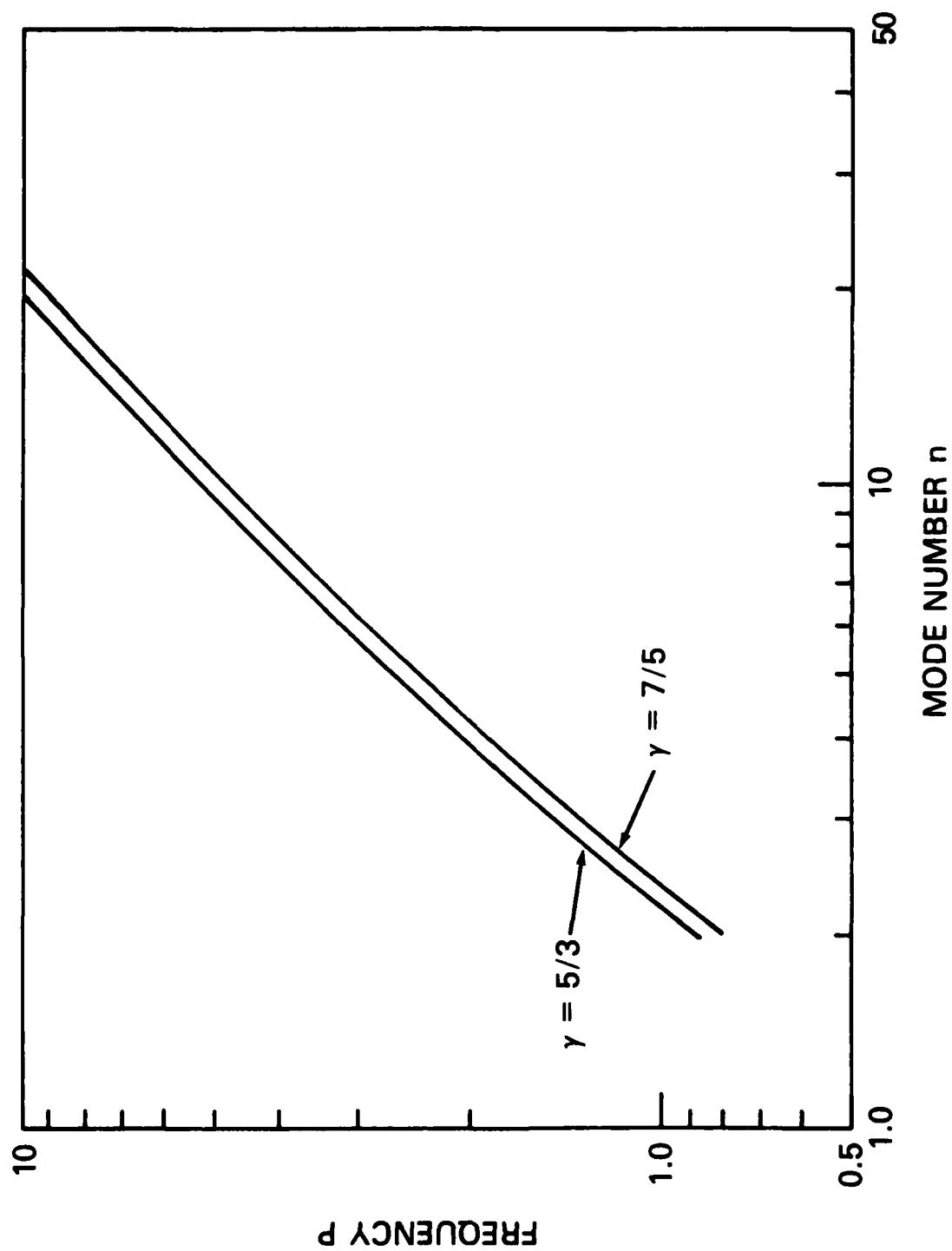


Fig. 2 — Oscillation frequency in \mathcal{E}_n of spherical harmonic perturbation of a spherical shock front as a function of mode number for a perfect gas with $\gamma=5/3$ and $\gamma=7/5$.

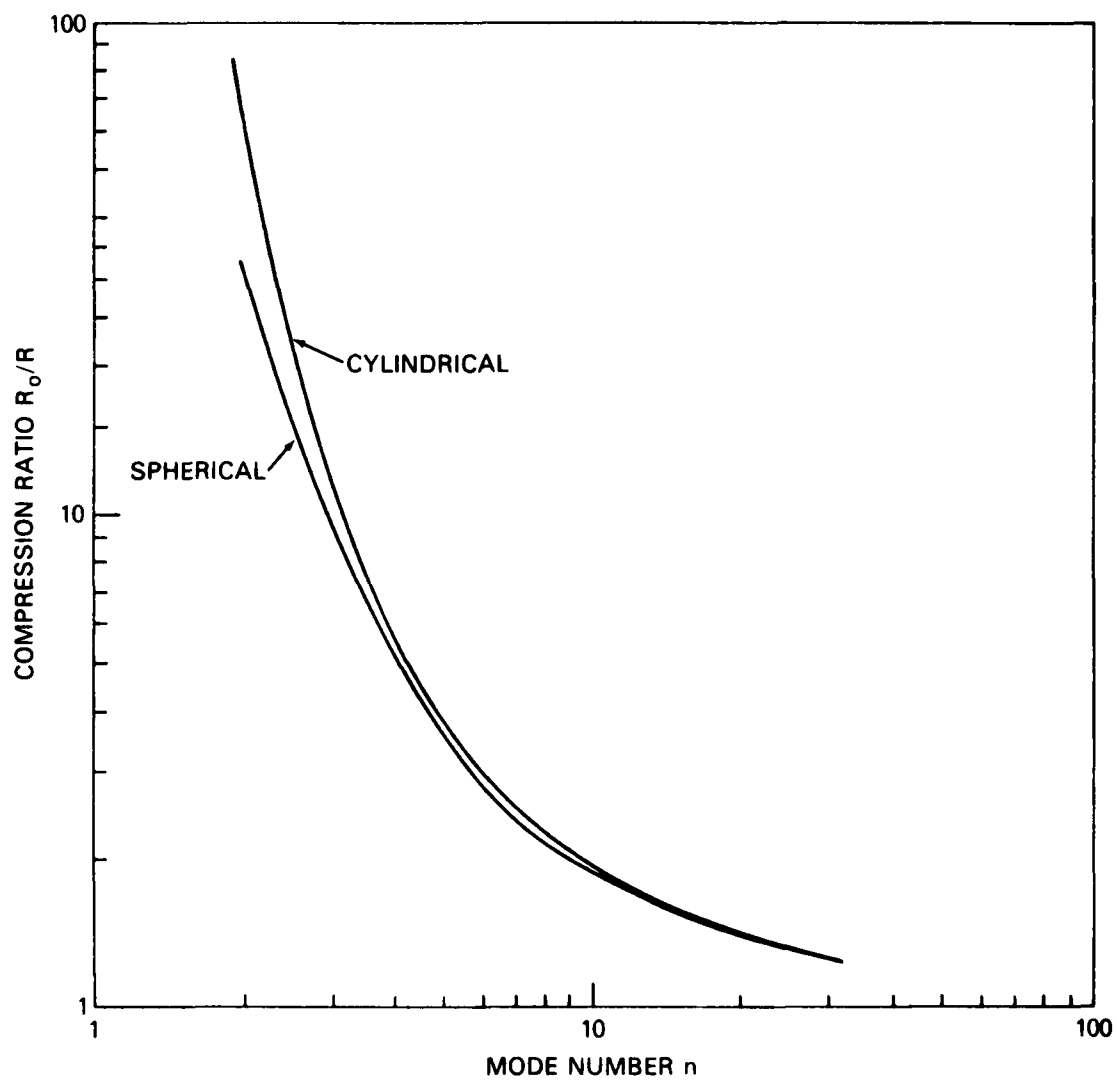


Fig. 3 — Compression ratio between successive minima in perturbation amplitude during perturbed shock collapse as a function of mode number.

IV. Numerical Integration

In order to assess the importance of nonlinear effects on the mode amplitude, the full nonlinear model equations were integrated with a code similar to that of Fong and Ahlborn (1979). The code advances the equations of motion of the shock front

$$\dot{\tilde{r}} = \tilde{v} ; \quad (43)$$

$$\frac{dM}{dA} = \frac{M^2 - 1}{\lambda(M) M A} , \quad (44)$$

either in plane coordinates (for cylindrical collapse viewed in a plane through the axis) or in cylindrical coordinates (for spherical collapse viewed in the equatorial plane).

The equation for the cross-sectional area is not integrated directly, but areas are taken from the kinematics of the integrated ray tubes. A second-order-accurate space-and-time-centered algorithm is employed to advance the grid locations and Mach numbers. Thus the problem of computing the shock shape is reduced to integrating a set of ordinary differential equations for the trajectories of a finite number of grid points located along the shock front, and for their associated time-dependent Mach numbers. The integration is subject to a timestep limit analogous to the Courant condition for the one-dimensional fluid equations. This algorithm allows for the propagation of so-called shock-shocks (discontinuities in the slope and Mach number of the shocks predicted by the Whitham theory) in either direction, since the scheme is centered and symmetric. The equations for the shock surface are analogous to the one-dimensional Lagrangian equation of motion, where the shock position takes the place of the fluid position, the ray tube area takes the place of fluid density, and the Mach

number takes the place of the fluid velocity. Thus many of the properties of one-dimensional motion, e.g., disturbances traveling along characteristic directions and nonlinear wave front steepening, show up in the shape of the shock surface.

It was found necessary to redistribute the grid points to prevent unacceptably short timesteps as the mesh points crowd together near the shock-shock regions. The algorithm diffuses the grid points a small amount parallel to the shock front in such a way as to make the distances between points more nearly equal. This diffusion plays a role similar to that of an artificial surface tension at interfaces.

To test the accuracy of the numerical procedure described above, we compared the results of the calculation with those predicted by the self-similar solutions for the collapse of an infinitely strong shock due to Guderley (1942). The self-similar solution predicts a shock position given by $R = C (-t)^\eta$ with $\eta = .717$ for a $\gamma = 1.4$ gas according to Guderley. This gives a shock Mach number as a function of radius

$$\dot{R} = -\eta C (-t)^{\eta-1} \sim R^{(\eta-1)/\eta} \quad (45)$$

Thus

$$M \sim R^{(\eta-1)/\eta} = R^{-.3947} \quad (46)$$

The C-C-W approximation for large M gives

$$\frac{dA}{A} = 2 \frac{dR}{R} = \left(1 + \frac{2}{\gamma+1} \frac{1-\sigma^2}{\sigma}\right) \frac{(2\sigma+1) M^2 + 1}{M^2 - 1} \frac{dM}{M} \quad (47)$$

with

$$\sigma = \left[\frac{\gamma-1}{2\gamma} \right]^{\frac{1}{2}}$$

This yields

$$M \sim R^{-\frac{2\gamma\sigma}{(2\sigma+1)(\gamma\sigma+1)}} = R^{-.3941} \quad (48)$$

The exponents agree with the analytic Guderley solution to within 0.0015. In Fig. 4 we show the results of these models for the spherical convergence of a shock with an initial Mach number of 57 at a radius of 0.112 cm. The solid line is the analytic result of the Guderley solution. The triangles are the numerical results of the C-C-W approximation using the code described above with 25 mesh points around a circle in cylindrical coordinates (describing a spherical implosion). Comparing the results along the axis with those perpendicular to the axis, we see that the shock remains spherical to better than 1% during the entire implosion and the Mach number reproduces the Guderley solution with less than 0.5% error.

Spherical Shock Collapse

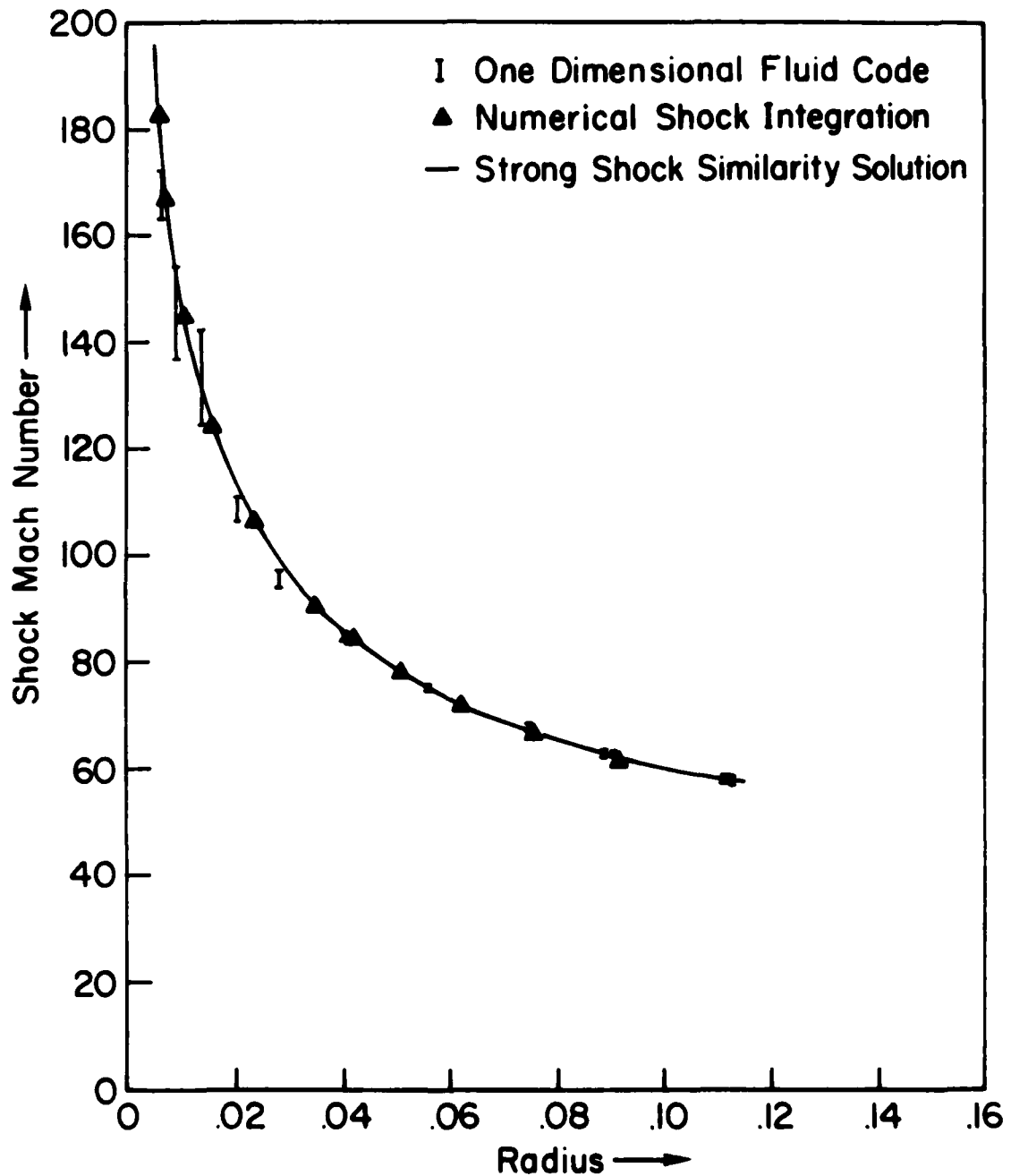


Fig. 4 — Comparison of analytic and numerical integration for self-similar spherical shock collapse (Guderley problem).

V. Comparison of Results of Linearized Model and Nonlinear Integration

In Fig. 5 and 6 we show the results of the analytic and numerical integration for mode numbers 2, 4, and 8 for cylindrical and spherical collapse. The solid lines are the analytic formulas and the circles show the numerical results. To insure beginning in the linear regime the initial amplitude of the modes was chosen such that $\zeta/r_0 = 10^{-3}$. Since the system of equations is second order in the perturbed shock location, both the amplitude and the velocity of perturbation must be specified. For these cases the velocity was chosen to be zero. This then uniquely determines the phase of the oscillation. The phase angle between the amplitude and the velocity is determined by the mode number and the specific heat ratios:

$$\varphi = \tan^{-1} \left[\frac{\lambda - \alpha}{2(\lambda + \alpha)p} \right] \quad (49)$$

Agreement appears very good until the mode amplitude becomes greater than a few percent. At this time nonlinear effects which can generate modes other than primary one drive the solution away from the linear result. Nonlinear steepening of the wave front generates higher order modes which begin to dominate the solution. In Fig. 7 we can see the form this takes. This figure shows the successive wave front shapes for an $l = 8$ spherical harmonic perturbation initialized with a large initial amplitude in order to show the effects of a large compression. As the shock collapses, the wave fronts begin to form cusplike-shapes in the region where the shock is left behind. For sufficiently large amplitudes a true cusp forms and the simple shock front no longer exists. It is replaced by a system of reflecting shock waves (see Fig. 8), which, however, are not treated in the present model. When this occurs a large portion of the shock energy can be left behind in the reflected shock system, thus decreasing the

compressional effect of the imploding shocks. Solutions of this type are referred to below as having kink instabilities in the shock front.

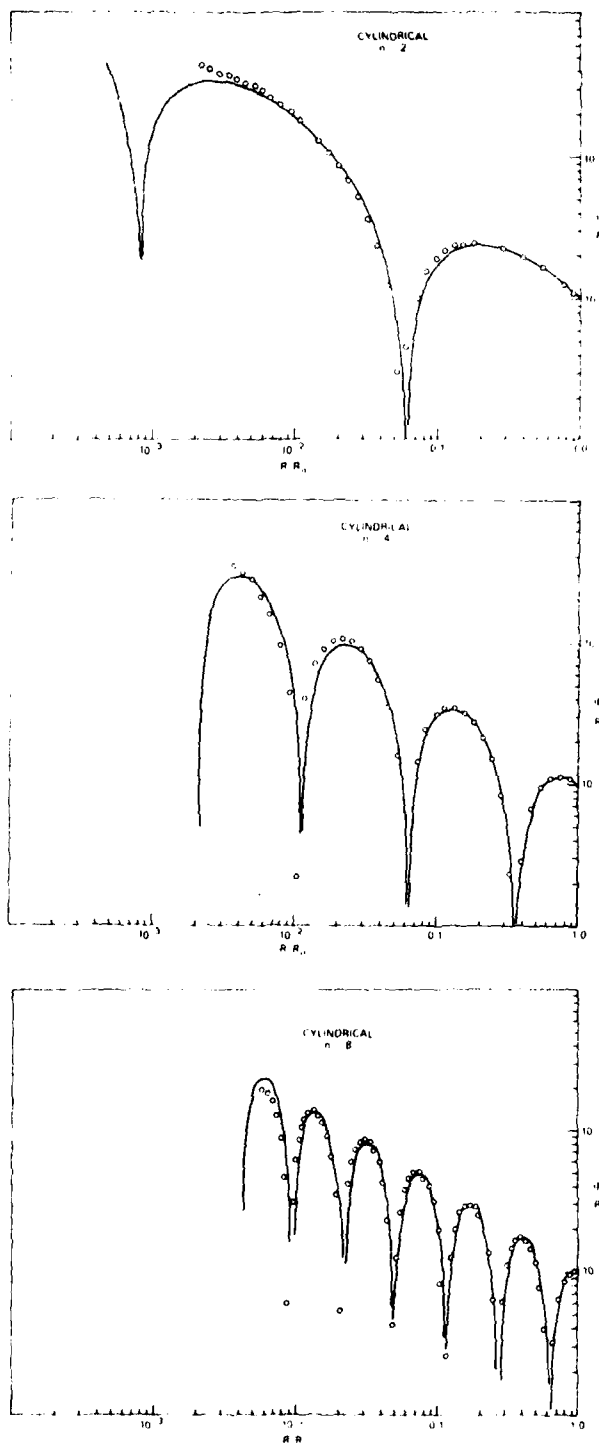


Fig. 5 — Comparison of analytic (solid lines) and numerical integration (open circles) for maximum perturbation amplitude as a function of radius for cylindrical shock collapse at three different mode numbers. Deviation at small radii is due to nonlinear effects not in analytic model.

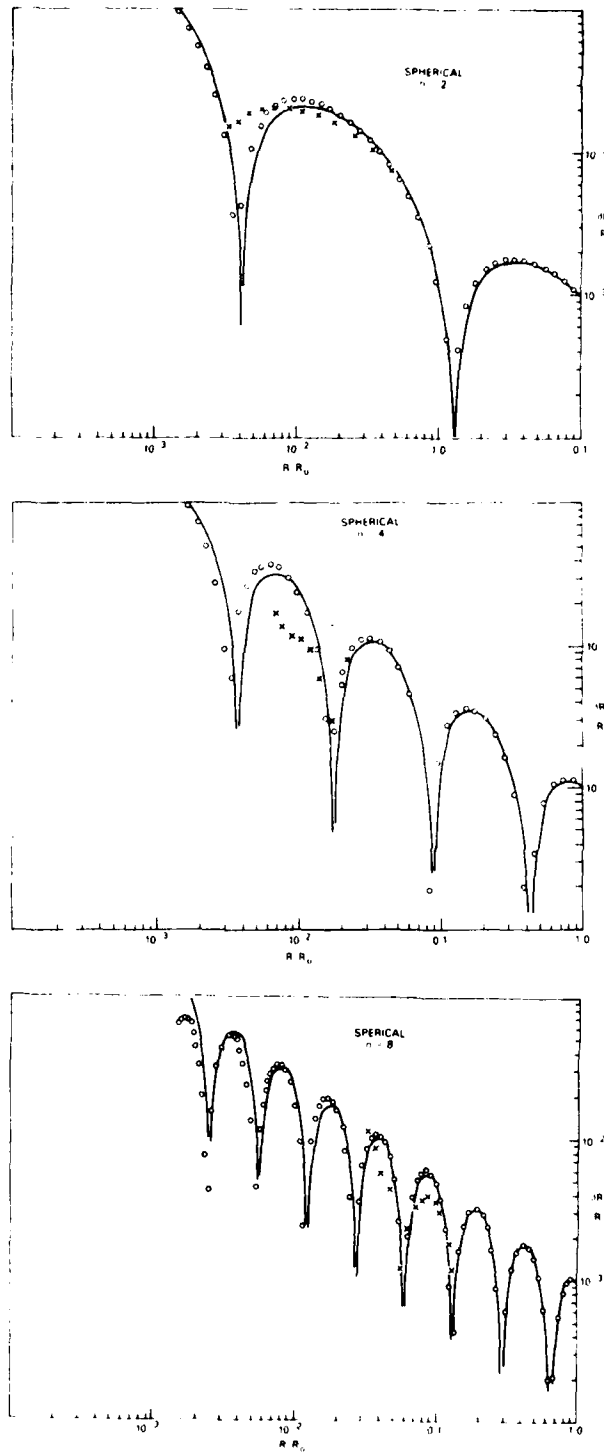


Fig. 6 — Comparison of analytic (solid lines) and numerical results (open circles) for spherical shock collapse for mode numbers 2, 4, and 8.

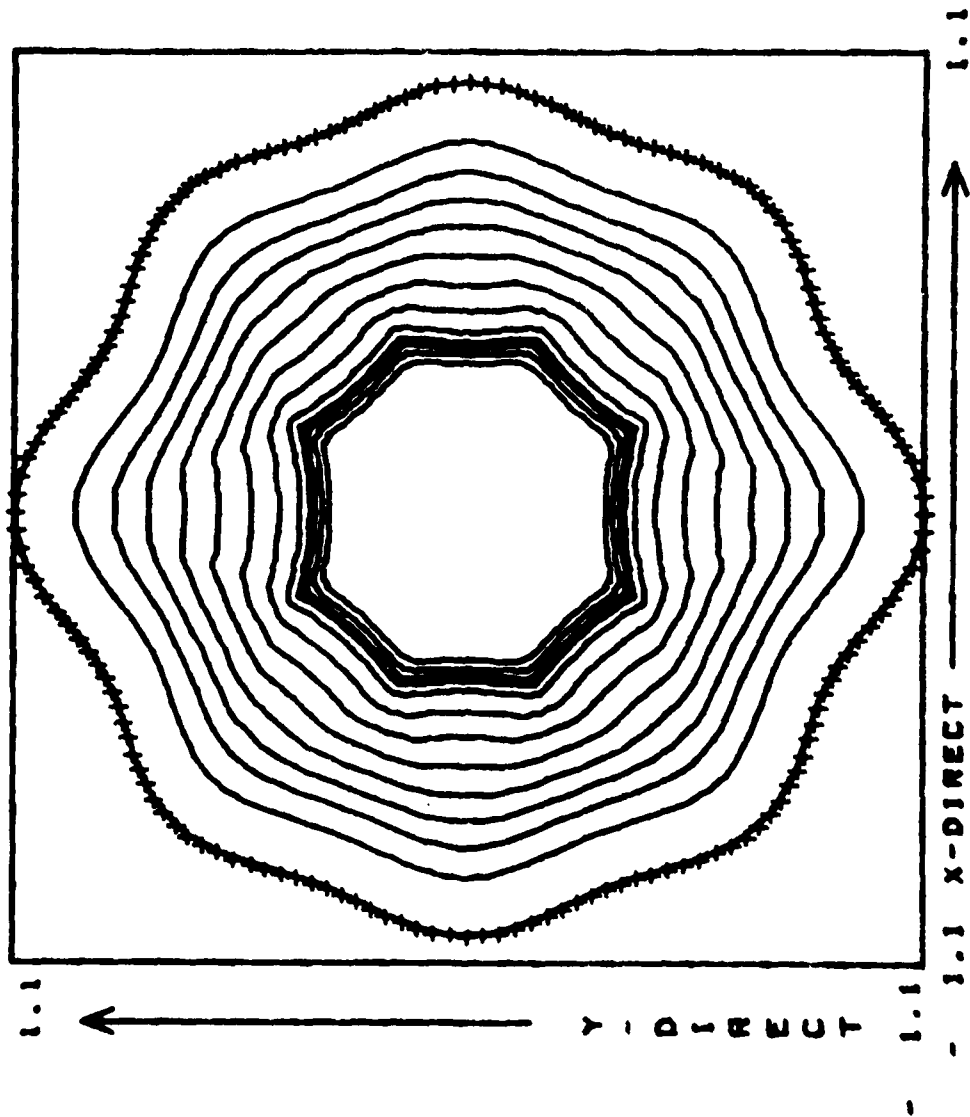


Fig. 7 — An example showing formation of cusp-line structure for large perturbation amplitudes in the nonlinear regime. Initial perturbation is a mode-number-8 Legendre polynomial with amplitude 10% of mean radius.

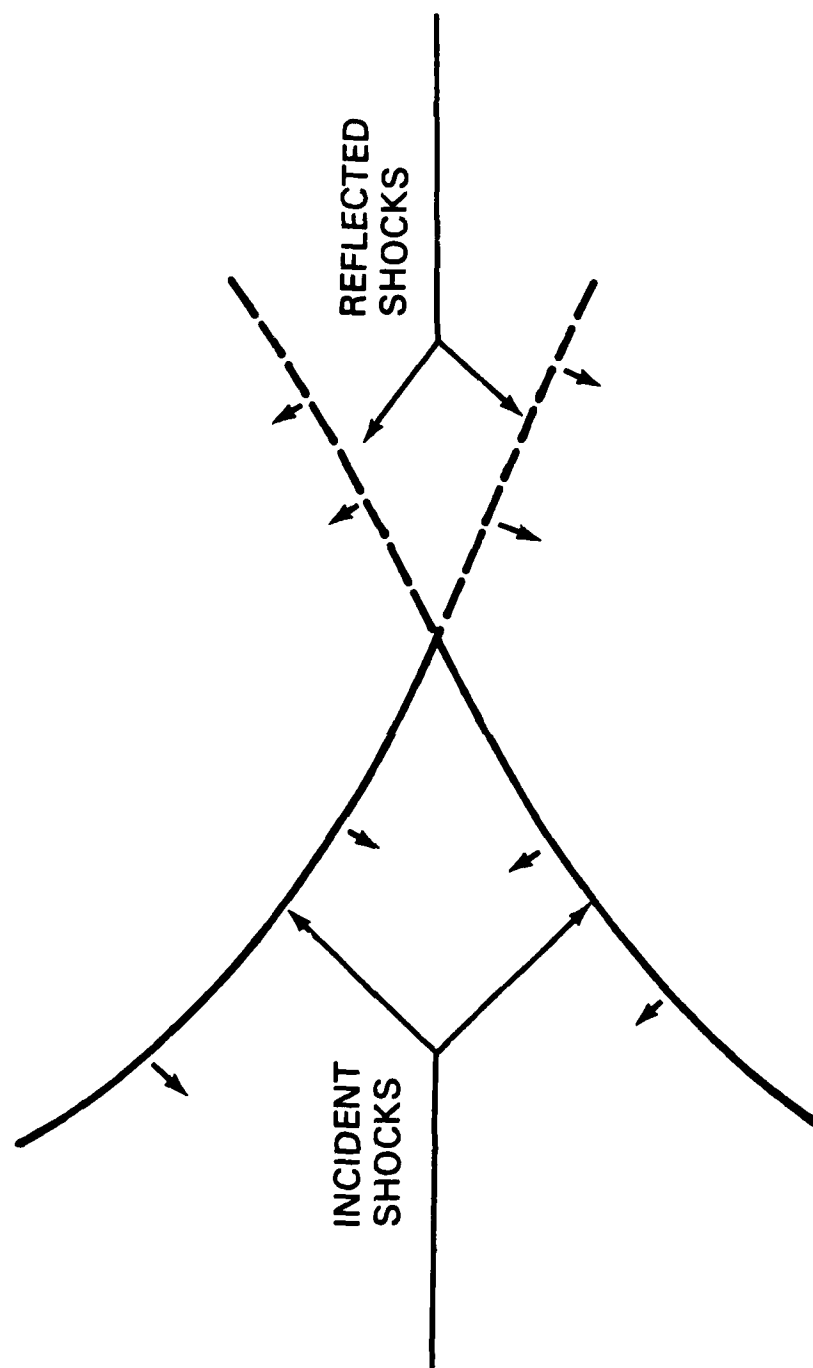


Fig. 8 — In the nonlinear regime shock-shocks are formed which are the intersections of regular of Mach reflections of shocks. This results in potential loss of shock energy in the reflected shock system.

VI. Nonlinear Modeling

In order to investigate more carefully how these kinks form and propagate, we look at perturbation in the form of a simple spherical cap of radius smaller than the initial mean shock radius. This shock cap intersects the main shock with an angle δ at a colatitude β , as shown in Fig. 9. For the purpose of this investigation the Mach number around the shock is assumed uniform at $M = 10$. In Fig. 10 we show the limits of stability for δ as a function of β . In addition we show the stability result in terms of $\delta r_0/r_0$ as a function of β ($\delta r_0/r_0$ is geometrically related to δ and β). When either δ or β becomes too large, the shock front is transformed into a nonlinear cusp-type regime instead of reverting to a more spherical form and oscillating. From Fig. 10b we can see that this is related to the initial perturbation and is a function of β . In each case instability is defined to occur if a cusp shock is formed before $r/r_0 < 10^{-2}$. This arbitrary definition is necessitated by the fact that all perturbations, given sufficient compression, eventually evolve into the cusp-shaped form. Realistically speaking, however, compressions of 10^6 are more than sufficient to achieve the compression and temperature rise necessary for ignition in pellet fusion.

Even for these single cap perturbations, oscillatory behavior is apparent for sufficiently small initial amplitudes. Let us compare the radius of the first minimum of the average deviation from a spherical or cylindrical shock for the cap perturbation to that for Legendre polynomial whose first zero forms the same angle as the β for the cap perturbation. We see from Fig. 11 that at least for smaller β (i.e., larger ℓ) the oscillation period is nearly the same. This indicates that the oscillation period (i.e., the

time or radius between minimum deviations from symmetric implosion) can be reasonably well predicted for arbitrary perturbations by matching to the lowest order Legendre polynomial which fits the perturbation. In Fig. 12 we show a stable case where the behavior about a nearly spherical implosion is oscillatory up to a compression of $r_0/r = 10$. In Fig. 13 we show an unstable case where a cusp is clearly forming after a single overshoot of the perturbation and a compression of $r_0/r = 4$.

From these results we see that two interdependent factors control when the nonlinear kinks will begin to form. One is the wavelength of the perturbation and the other is the angle at which the perturbation intersects the mean radius. The smaller the wavelength, the larger the angle that is tolerable. Note, however, that this angle and the mode amplitude are not independent. In terms of amplitude, the shorter the wavelength, the smaller the amplitude of disturbance that can be tolerated.

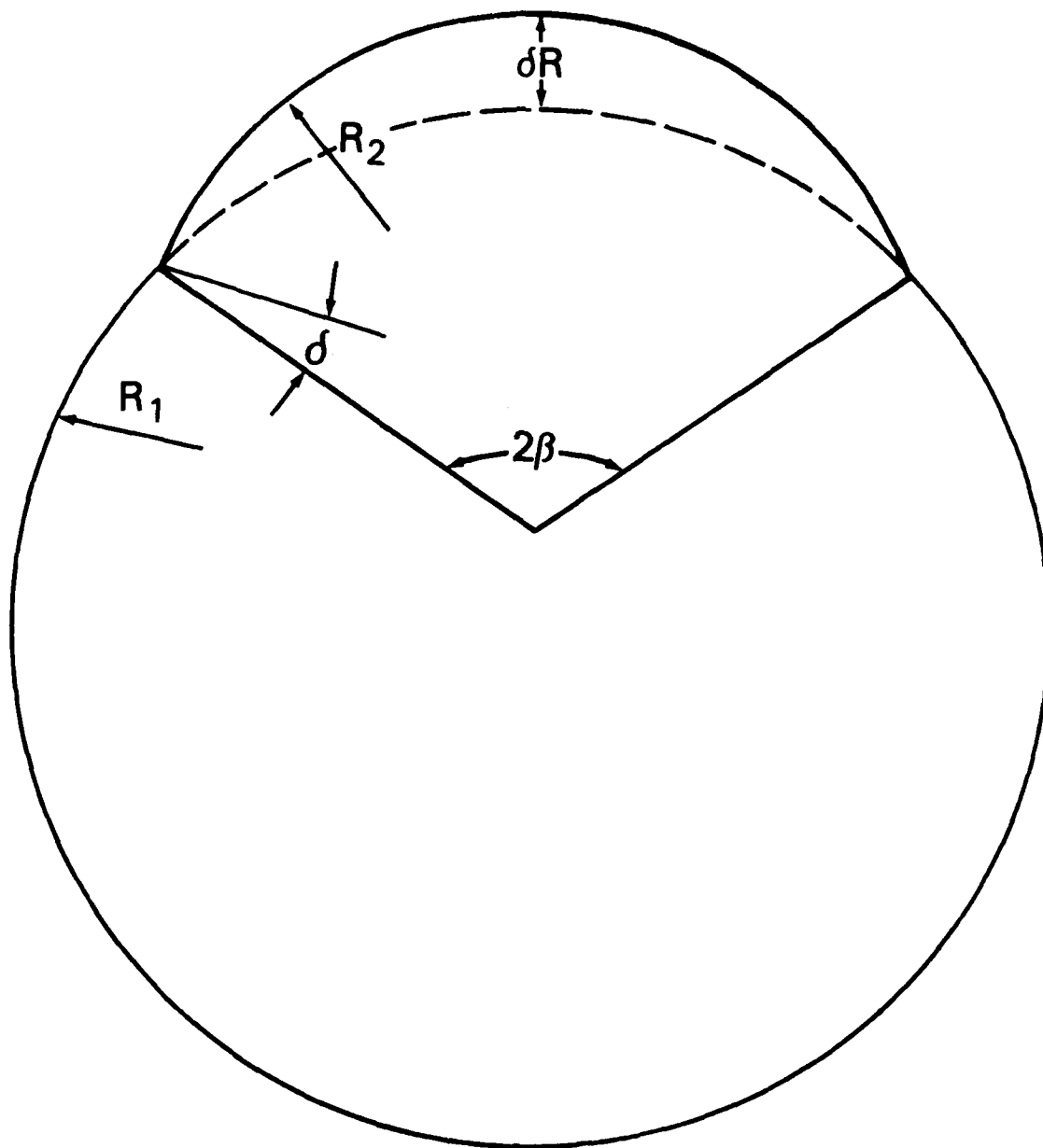


Fig. 9 — Initial perturbation of a spherical shock may be represented in terms of a cap at one pole with a radius of curvature smaller than the main shock. The perturbation magnitude δR , intersection half-angle β , and deviation angle δ are related by geometry.

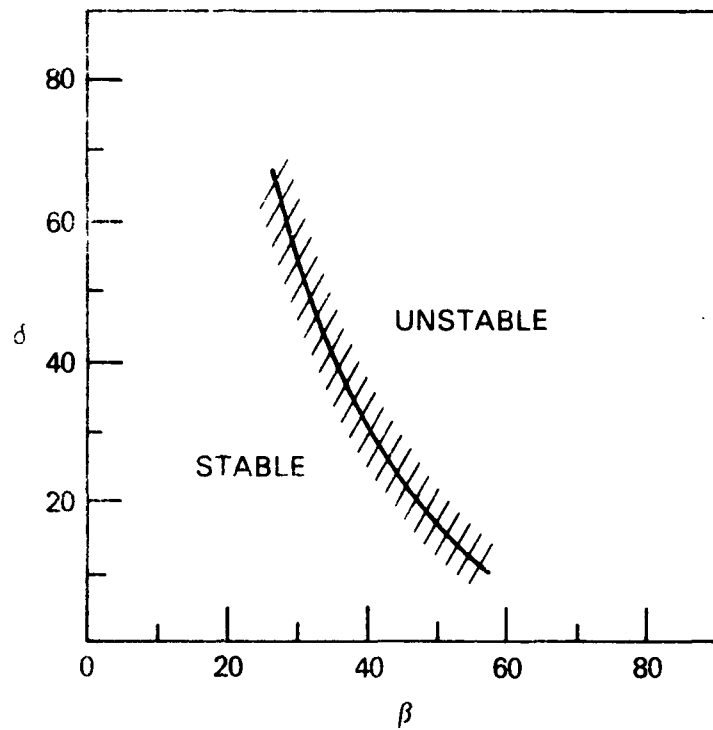


Fig. 10(a) — Stability limits for the spherical cap perturbation are given as a function of the deviation δ and intersection angle β as defined in Fig. 9. Instability is defined to occur when a kink forms before a compression radius $R/R_0 < 0.01$.

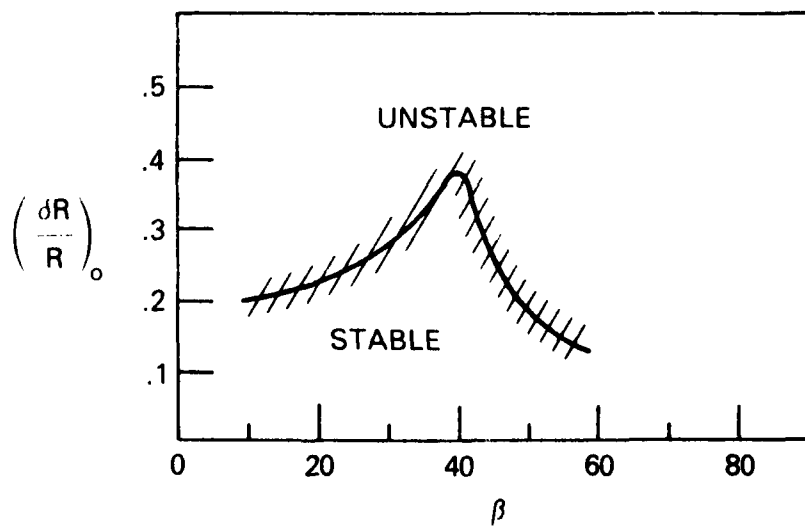


Fig. 10(b) — Stability limits are shown as a function of $(\delta R/R)_0$ and β . These two graphs are connected by simple geometric relations.

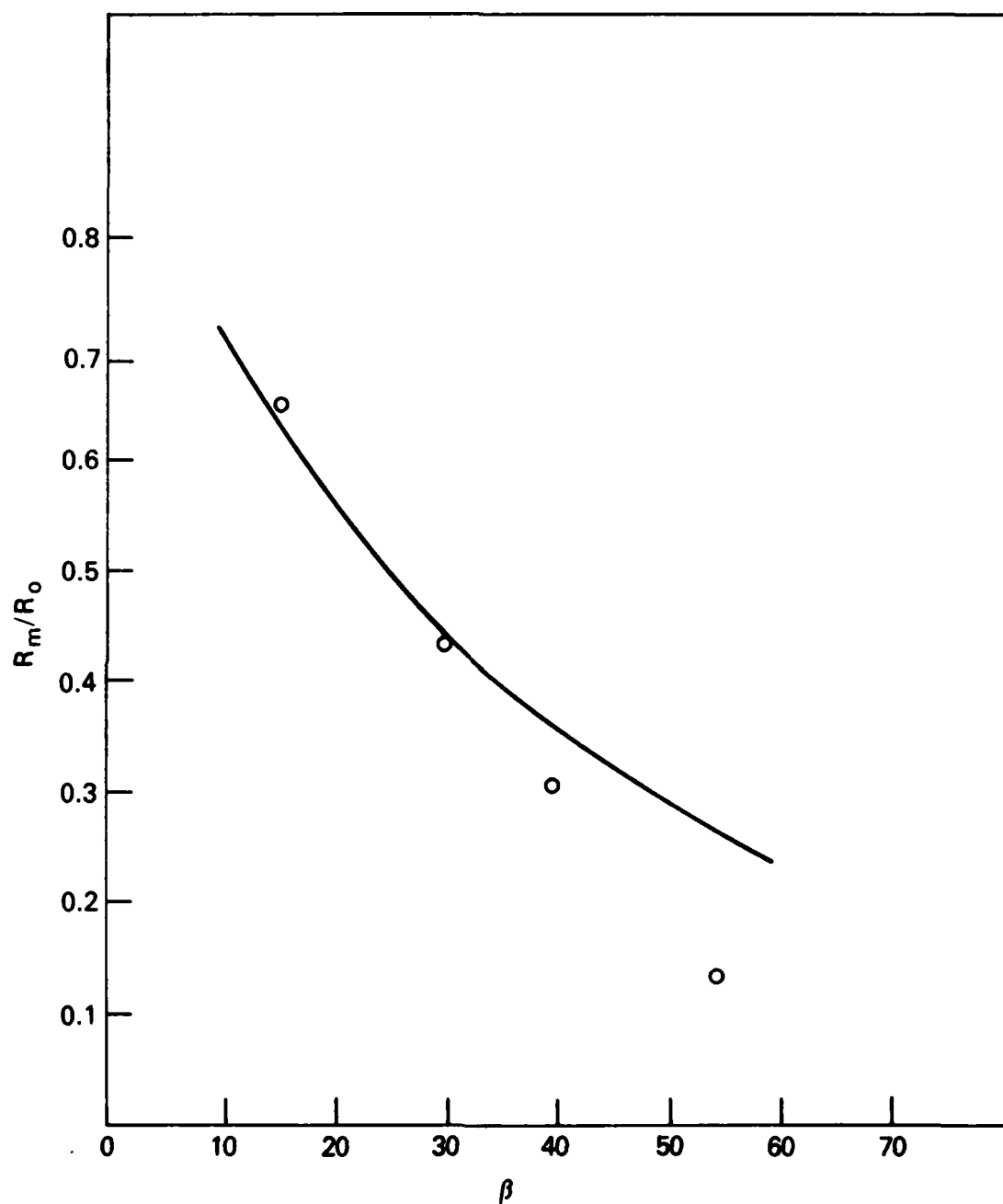


Fig. 11 — Compression ratio at the first minimum of $\delta R/R$ as a function of intersection angle. Open circles represent results obtained with Legendre polynomials, where β is the angle to the first zero.

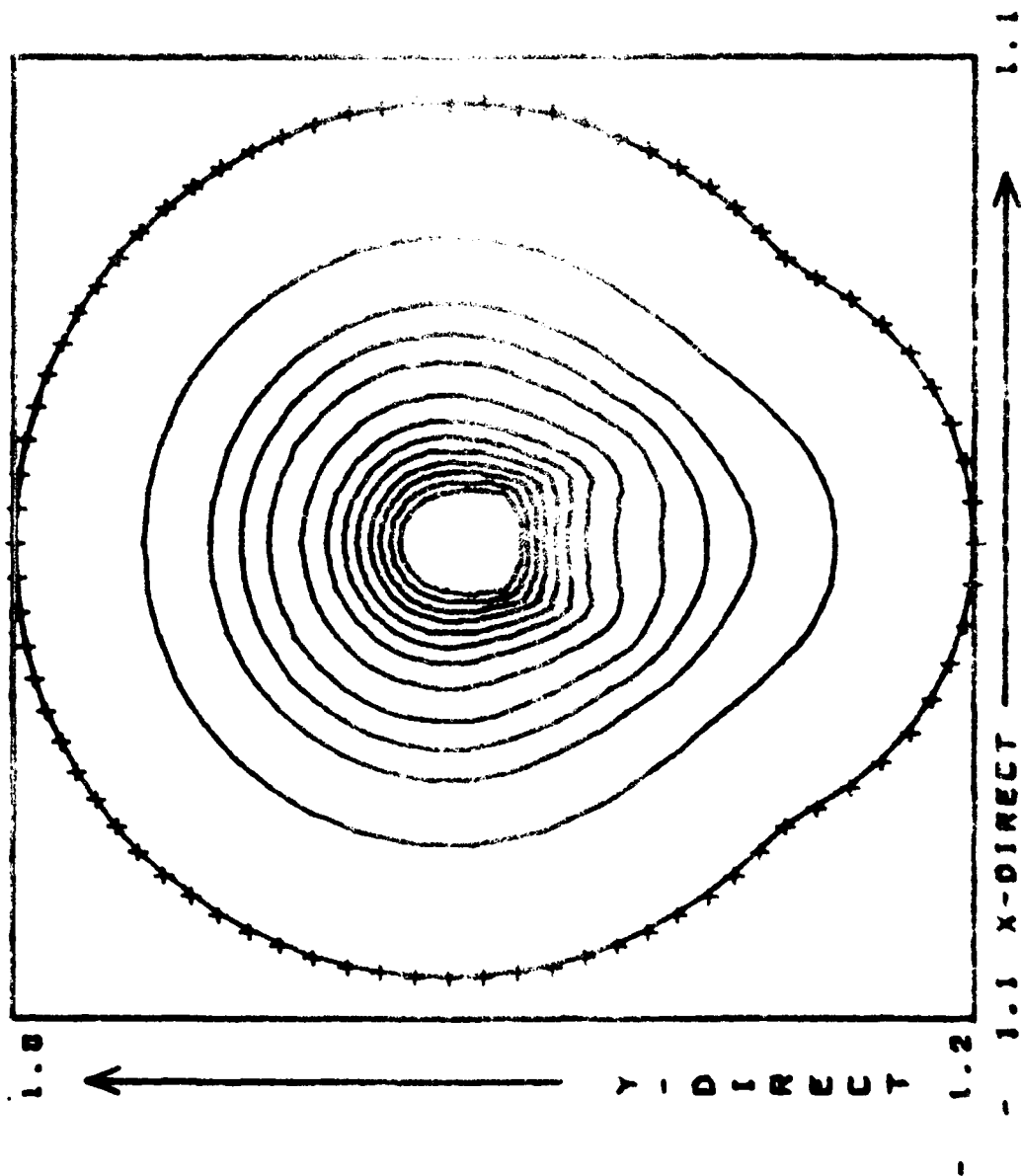


Fig. 12 -- Example of stable spherical cap perturbation where the solution oscillates and tends to become more spherical. No kinks appear before $R/R_0 < 0.01$, ($\alpha = 29^\circ$, $\beta = 39^\circ$, $\delta R/R = 0.2$).

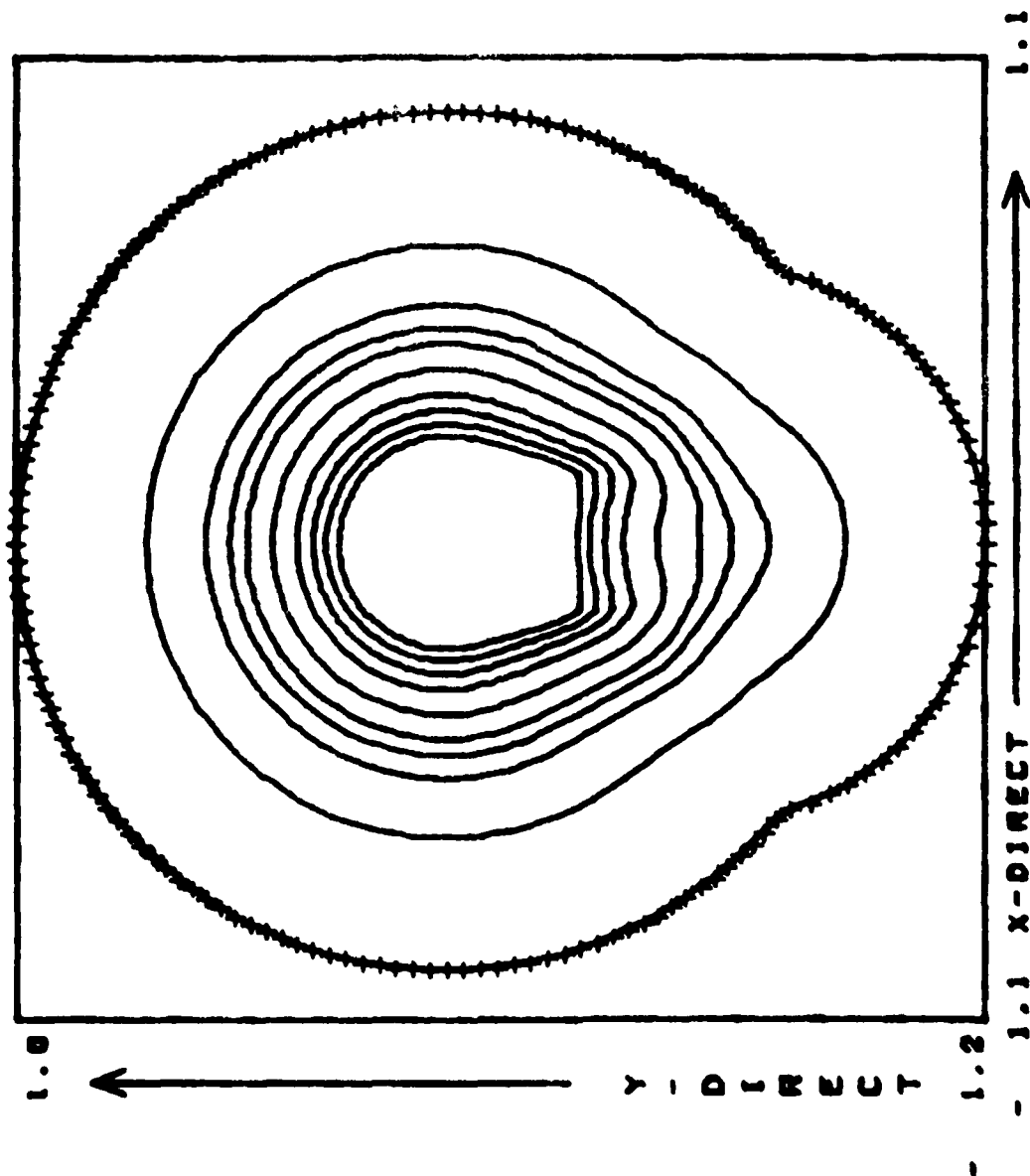


Fig. 13 — Example of an unstable spherical cap perturbation where kink instability forms after one oscillation. ($\alpha=39^\circ$, $\beta=34^\circ$, $\delta R/R=0.25$)

VII. Effect of density variation

Equation (1) was derived assuming a uniform density and temperature ahead of the shocks. The C-C-W methodology does not require the medium ahead of the shocks to be uniform, and we shall now investigate the effect a non-zero density variation in the undisturbed medium. However, we do not allow the density to increase rapidly enough that the shock decelerates. This would violate the important assumption that returning characteristics are negligible.

The compatibility relation along the inward-directed characteristic is given by

$$dp + \rho a du + \frac{\rho a^2}{u+a} \frac{dA}{A} = 0, \quad (50)$$

while the Hugoniot relations behind a strong shock ($M \rightarrow \infty$) are given by

$$\begin{aligned} u &= \frac{2}{\gamma+1} v; \\ p &= \frac{2}{\gamma+1} \bar{\rho} v^2 = \bar{\rho} u v; \\ \rho &= \frac{\gamma+1}{\gamma-1} \bar{\rho}; \\ a^2 &= \frac{\gamma p}{\rho} = \frac{2\gamma(\gamma-1)}{(\gamma+1)^2} v^2, \end{aligned} \quad (51)$$

where u is the fluid velocity behind the shock, p is the pressure behind the shock, ρ is the density behind the shock, and $\bar{\rho}$ is the undisturbed density. Differentiating the relation for p we get

$$dp = \frac{2}{\gamma+1} v^2 d\bar{\rho} + \frac{4}{\gamma+1} \bar{\rho} v dv. \quad (52)$$

Combining Eqs. (50-52) we have

$$\frac{2}{\gamma+1} v^2 d\bar{\rho} + \left(\frac{4}{\gamma+1} + \frac{2}{\gamma+1} \sqrt{\frac{2\gamma}{\gamma-1}}\right) \bar{\rho} v dv + \frac{4\gamma}{[2(\gamma+1) + \sqrt{2(\gamma-1)}]} \bar{\rho} v^2 \frac{dA}{A}, \quad (53)$$

or

$$\frac{dv}{v} = - \left(\frac{\gamma+2}{\gamma} + \sqrt{\frac{2\gamma}{\gamma-1}}\right)^{-1} \frac{dA}{A} - (2 \sqrt{\frac{2\gamma}{\gamma-1}})^{-1} \frac{d\bar{\rho}}{\bar{\rho}}. \quad (54)$$

If we now write this in the form of Eq. (7) we have

$$\lambda (\dot{v}/v) = -\dot{A}/A - \kappa \frac{\dot{\bar{\rho}}}{\bar{\rho}}. \quad (55)$$

Using Eqs. (4), (6) and (10) and the relation

$$\frac{\dot{\bar{\rho}}}{\bar{\rho}} = \underline{v} \cdot \nabla \bar{\rho}, \quad (56)$$

we have

$$(\lambda/v) \dot{=} \nabla \cdot \underline{n} + \kappa \underline{n} \cdot \nabla \ln \bar{\rho}. \quad (57)$$

Assuming a density profile of the form $\bar{\rho} \sim r^{-q}$ the zeroth order symmetric equation becomes similar to Eq. (15),

$$(\lambda/\dot{r}) \dot{=} (\alpha - \kappa)/r. \quad (58)$$

This has a solution analogous to Eq. (18),

$$r = R (\omega t)^{\lambda / (\lambda + \alpha - \epsilon q)} \quad (59)$$

The effect of a positive q (density increasing toward the axis) is to cause the shock to accelerate more slowly than the $q=0$ case. (A negative q will cause the shock to accelerate faster).

Again linearizing the equations as in Section 2, we have to first order

$$\begin{aligned} (-\lambda v_1 / v_0^2) = \nabla_0 \cdot \underline{n}_1 - (\nabla_0 \underline{\xi}) : (\nabla_0 \underline{n}_0) + [\kappa \underline{n}_1 \cdot \nabla_0 \ln \bar{\rho} \\ - \underline{n}_0 \cdot (\nabla \underline{\xi}) + \nabla_0 \ln \bar{\rho} + \underline{n}_0 \cdot \nabla_0 (\underline{\xi} \cdot \nabla_0 \ln \bar{\rho})] \end{aligned} \quad (60)$$

Using vector manipulations similar to those in Section 2, we obtain

$$\begin{aligned} -(\lambda \underline{n}_0 \cdot \underline{\xi} / v_0^2) = -\nabla_0 \cdot [(I - \underline{n}_0 \underline{n}_0) \cdot \nabla (\underline{n}_0 \cdot \underline{\xi})] + \underline{\xi} \cdot \nabla_0 (\alpha / r_0) + \\ \underline{n}_0 \underline{\xi} : \nabla_0 \nabla_0 \ln \bar{\rho} . \end{aligned} \quad (61)$$

The last term of Eq. (61) adds an additional term to Eq. (29), given by

$$\underline{n}_0 \underline{\xi} : \nabla_0 \nabla_0 \ln \bar{\rho} = \zeta (\ln \bar{\rho})'', \quad (62)$$

where the double prime indicates a derivative with respect to r_0 .

Thus Eq. (61) becomes

$$- (\lambda \dot{\zeta} / v_0^2) = (Q - \alpha + \kappa q) \zeta / r_0^2 \quad (63)$$

Now from Eq. (53) we get

$$\frac{d \ln v_0}{dr_0} = - \frac{\alpha - \kappa q}{\lambda} r_0^{-1}, \quad (64)$$

and using Eq. (30) we have after a little algebraic manipulation

$$\lambda \frac{d^2 \zeta}{dr_0^2} + \frac{\alpha - \kappa q}{r_0} \frac{d\zeta}{dr_0} + \frac{Q - \alpha + \kappa q}{r_0^2} \zeta = 0. \quad (65)$$

The resulting indicial equation is

$$\lambda \beta (\beta - 1) + (\alpha - \kappa q) \beta + (Q - \alpha + \kappa q) = 0, \quad (66)$$

or

$$\beta = \frac{(\alpha - \alpha + \kappa q) \pm [(\alpha - \alpha + \kappa q)^2 - 4\lambda Q]}{2\lambda}. \quad (67)$$

We note from this result that the effect of including density variation is found to first order by replacing everywhere the term α by $\alpha - \kappa q$. That is, the acceleration normally due to the geometric factor α is modified by an additional term κq related to the acceleration caused by a density variation. Positive q (density increasing toward the axis) has the effect of reducing the acceleration due to geometric convergence. For sufficiently large q the acceleration vanishes. This situation, however, violates the

assumption in the C-C-W model that the shock system is accelerating. The ratio of the disturbance amplitude to the zeroth-order radius continues to satisfy $\zeta/r_0 \sim t^{-1/2}$, with the frequency appropriately modified. In terms of the zeroth order radius, however, the growth becomes $\zeta/r_0 \sim r_0^{-(\lambda+\alpha-\kappa q)/(2\lambda)}$. A positive q thus decreases the relative growth of the shock perturbation as a function of the shock radius.

VIII. Conclusions

The C-C-W approximation, which appears to be very accurate for computing converging shock waves, predicts that the converging shock is always unstable, in the sense that the ratio of the perturbation size to the average radius diverges at the time of collapse. The cylindrical and spherical cases differ only quantitatively. The growth rate is only a power law, however, and therefore is not as serious as an exponential growth. For mode number greater than unity, the perturbations oscillate in $\ln t$ with a mode-number-dependent period. The amplitude growth, however, is independent of mode number.

For sufficiently large amplitude the linear behavior breaks down and the solution develops nonlinearly into a kink form, where a reflected shock is left behind in the material, serving as a potential loss of shock energy in the collapsing shock.

REFERENCES

- Bernstein, I. B., and Book, D. L., Ap. J. 225, 633 (1978)
- Chester, W. (1954) Philos. Mag. 45, 1293
- Chisnell, R. F. (1955) Proc. R. Soc. London Ser. A 232, 350
- Guderley, G. (1942) Luftfahrtforschung 18, 302
- Fong, K. and Ahlborn, B. (1979) Phys. Fluids 22 (3), 416
- Whitham, G. B. (1957) J. Fluid Mech. 2, 146
- Whitham, G. B. (1958) J. Fluid Mech. 4, 337

**DATA
FILM**